

Total Dose Testing of a CMOS Charged Particle Spectrometer]

B.R. Hancock, *Member, IEEE* and G.A. Soli²

Jet Propulsion Laboratory
California Institute of Technology
Pasadena, CA 91109

Abstract

A first-generation CMOS Charged Particle Spectrometer chip [1] was designed at JPL for flight on the STRV-2 spacecraft. These devices will collect electron and proton spectra in low Earth orbit as part of an experiment to demonstrate Active Pixel Sensor (APS) technology in space. This paper presents the results of total dose testing on these chips and, where possible, attempts to extend the results to other Active Pixel Sensors.

I. INTRODUCTION

CMOS charged particle spectrometers have been proposed [1] as a candidate for measuring space particle environments. These devices, which are a form of Active Pixel Sensor (APS), are fabricated in a standard CMOS process and have a variety of advantages. Integrated analog processing, digital control circuitry and a single 5 V power supply provide easy interfacing, resulting in a compact, powerful instrument.

A first-generation CMOS Charged Particle Spectrometer chip, designated CPS32, was designed at JPL for flight on the STRV-2 spacecraft, as part of an experiment to demonstrate APS technology in space. A collection of CPS32 chips will be used to measure the energy spectra of trapped electrons and protons in STRV-2's low earth orbit, while a pinhole camera will allow simultaneous collection of angular information for low energy electrons. This capability is made possible by the pixellation of the detector, and its easy digital interfacing.

During the 1-year mission, these devices will be exposed to an estimated dose of 10 krad (100 Gy), from a mixture of trapped protons and electrons. They will be required to operate at unregulated ambient temperatures, expected to vary between -40°C and +60°C. This paper presents the results of total dose testing of these chips with a Co⁶⁰ gamma source. Due to funding limitations, we were not able to perform displacement damage testing using protons. However, the results obtained here indicate that the total dose effects will predominate. Where possible, an attempt is made to extend the results to other APS applications.

¹The research described in this paper was carried out by the Jet Propulsion Laboratory, California Institute of Technology, under a contract with the National Aeronautics and Space Administration

²Present address: Scientific Imaging Technologies, Inc., Beaverton, OR 57075.

H. DESIGN OF THE CPS32

A. Architecture

Fig. 1 shows the overall architecture of the CPS32. The sensor portion of the chip consists of a 32x32 array of pixels on 26.4µm centers, with each pixel containing a 9.6µm x 13.2µm p-n diode detector, an amplifier and a multiplexer switch to the column bus. The outputs of the columns are multiplexed to an output buffer, and address decoding is performed by digital support circuits. This constitutes a basic Active Pixel Sensor. The chips were fabricated through the MOSIS fabrication service using the 1.2µm Hewlett-Packard n-well process. This is a standard, commercial CMOS process with LOCOS isolation, an unhardened 21 nm gate oxide, and a 500 nm field oxide.

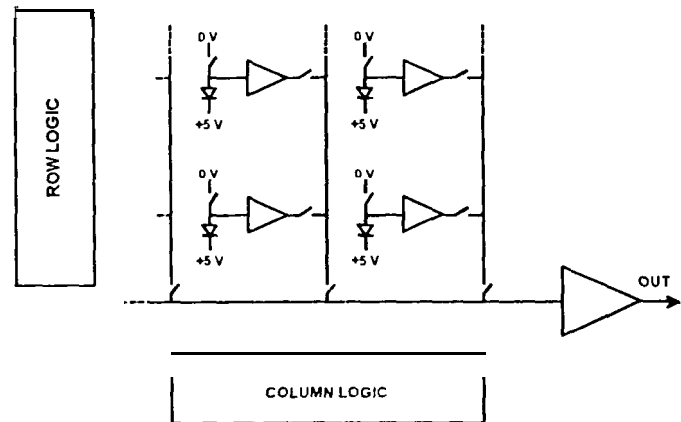


Figure 1: The architecture of the CPS32

Figure 2 shows a more detailed representation of the signal path from the detector to the output. The detector is reset by a transistor switch, buffered by a source follower, and connected to the column bus by another transistor switch. Selection and reset are performed on a row-by-row basis. A transistor at the bottom of each column, biased by a fixed external bias, serves as a load to the selected pixel. Finally, a column multiplexer connects the desired signal to a common output source follower. Note that the pixel and column circuitry is entirely p-channel, while the output buffer is n-channel.

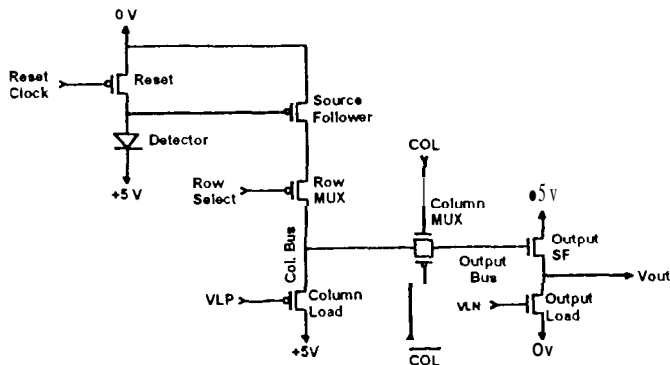


Figure 2: The CPS32 signal path.

In addition to the basic detector array, the CPS32 also includes pFET dosimeters [2] to measure total dose, and has additional multiplexer channels for the dosimeters and an external temperature sensor.

Because this was a first generation design, the design was kept simple, and many features were not optimized. This reduced the development risk, and allowed flexibility in selecting the operational mode. The digital logic, for example, is very simple, consisting only of address decoders. More advanced designs would include circuitry to generate all the clocking signals, and might include event discrimination to reduce the load on the instrument processor.

The analog processing in the CPS32 is likewise simple. While other APS designs [3] incorporate storage capacitors at the bottom of each column to facilitate correlated double sampling (CDS) or signal-minus-reset processing [4], these were not used for the CPS32 because the capacitors were expected to be sensitive to particle events. This would interfere with particle spectrometry, where the desired signal consists of a few events in an otherwise dark background. Such interference also occurs in APS imagers (and all other imagers as well), but it generally represents a small fraction of the data and is either ignored or removed by image processing.

B. operation

In operation, the pixels are reset, one row at a time, by turning on the reset transistors. This places a reverse bias on the detector diodes. Any charge generated during the integration time, due to particle events, photocurrent or dark current, will be integrated on the diode capacitance. At the end of the integration time, the pixels are sequentially selected for read out. Because of the buffering provided by the source followers, the readout can be non-destructive, allowing signal processing functions such as correlated double sampling and multiple sampling [5]. Even with the simple built in digital circuitry, the only timing signals needed are the row and column addresses and the reset clock.

C. Comparison to IR Multiplexers

The design of the CPS32, as described above, is identical that of a standard source-follower-per-detector (SFD) infrared multiplexer [4]. There are, however, significant differences from a radiation perspective. First, the detectors in the CPS32 are monolithically integrated diodes, rather than separate infrared detectors. Therefore, the radiation hardness of the detectors is limited to that which can be obtained within the CMOS process.

The main difference, however, is in the operating temperatures. Narrow bandgap infrared detectors need to be operated at cryogenic temperatures to reduce their dark current, and so the multiplexer are also operated cold. This significantly changes the physics of the radiation effects. Additionally, any dark current sources generated in the silicon multiplexer will be frozen out. In contrast, the CPS32 will be operated at ambient temperatures. The testing reported here was performed at temperatures between -25°C and $+25^{\circ}\text{C}$, with radiation exposures at room temperature.

D. Design Features for Radiation Hardness

The CPS32 pixels contain two design features intended to improve the radiation hardness. First, p-channel transistors were chosen for the pixels, with diodes fabricated as p^+ diffusions in the n-well. This was motivated by the fact that p-channel transistors are generally reported to have lower densities of radiation induced interface states which, in turn, should result in lower increases in dark current, P-channel transistors are also not subject to radiation induced inversion in the field oxide and bird's-beak region, nor to the increases in sub-threshold leakage seen in n-channel transistors. Such leakage would be disastrous to the charge-sensitive front end of the CPS32. Only the digital logic, the column multiplexer, and the output amplifier contain n-channel transistors, and these are all low-impedance circuits.

The second feature for radiation hardness, shown in Figure 3, is the use of an annular reset transistor, enclosing the detector diode. This fully isolates the diode, the most sensitive portion of the circuit from any possible bird's-beak or field oxide leakage. It also means that the diode depletion region intersects the silicon surface under gate oxide, rather than under the bird's-beak, which has a higher concentration of interface states.

There are, however, some consequences of these special radiation-hardening features. The use of diodes in the n-well means that the collecting volume is thin, as shown in Figure 3. In fact, the collecting volume is only about half the well depth, since charge generated in the lower region of the well is collected by the power supply at the substrate junction and is not sensed. Therefore, the detector measures the charge density along the track, i.e. the LET of the particles.

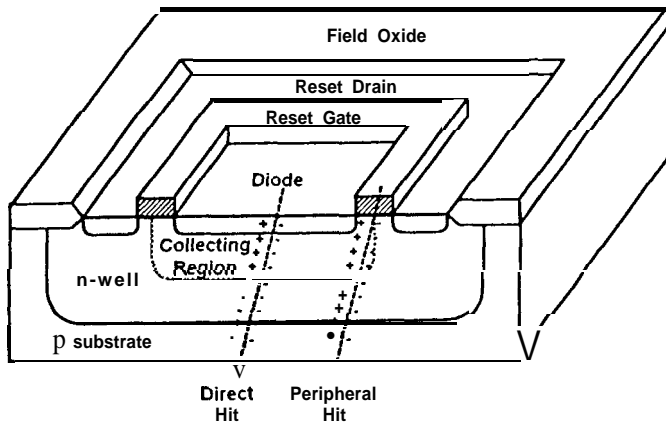


Figure 3: Cross section of the CPS32 pixel (not to scale). Note the thin collecting volume and the peripheral hit regions.

MOSIS does not report the well parameters that would be needed to predict device sensitivity. However, from the alpha particle sensitivity reported in Section IV, we determine that the effective collecting region is $1.2 \mu\text{m}$ thick, while capacitance values indicate a well doping level of $\sim 2 \cdot 10^{17} \text{ cm}^{-3}$. Both of these values are physically reasonable and imply efficient collection of the radiation-generated carriers. Although the thin collecting region results in a small signal charge, this is compensated for by the high conversion gain of the CPS32.

The use of the annular geometry results in a very wide reset transistor, with a high gate-to-source capacitance. This produces a large clock feedthrough and reduces the dynamic range. However, the annular transistor and thin collecting layer have advantages in reducing the problem of peripheral hits, discussed below.

E. Performance Characteristics

The primary performance parameter for an APS, whether used for charged particle spectrometry or for imaging, is the signal-to-noise ratio. The signal level for the CPS32 is relatively high, due to the small sense-node capacitance of $\sim 70 \text{ fF}$, which is dominated by the diode. This is a consequence of breaking the detector area into small pixels, and is particularly advantageous for charged particle spectrometry, where the signal charge is independent of the pixel size and integration time.

The noise can be divided into spatial, temporal and detection components. The spatial, or fixed pattern noise (FPN), is generally the largest, consisting of variations in offset and gain from pixel to pixel. Offset variations are the result of pixel-to-pixel differences in transistor threshold voltages, clock feedthrough and dark current, while gain variations come from differences in transistor and diode parameters, notably physical dimensions and doping levels.

Temporal noise, likewise, comes from various sources. Dark current, in addition to its spatial variation, also contains temporal variations. This is usually modeled as shot noise, and is a major driver for reducing the dark current. However, as described in Section IV, we have observed an additional temporal noise in the dark current, in the form of Random Telegraph Signals.

White noise and $1/f$ noise come from the pixel and output source followers, and from the measurement system. The $1/f$ noise is particularly a problem in a photodiode APS, like the CPS32, since it is not significantly reduced by correlated double sampling, as it is in a CCD or photogate APS. This is because the measurements of the relaxed reset level and the signal level must be separated by the integration time.

Reset noise, also called kTC noise, is a fundamental thermodynamic noise in the charge on the sense node capacitance after reset, equal to $-100 e$ for the CPS32. Reset noise is removed by the standard technique of correlated double sampling (CDS), which has the added advantage of removing the fixed offset components of FPN.

Detection noise is due to variability in the charge generation and detection processes. The variability of the charge generation is described by the Fano noise [6], which is a fundamental characteristic of the interaction of the particles with silicon, but it is not a significant component of the CPS32 noise. Variability of the collection process occurs because the division of collection between the two junctions is probabilistic, leading to a shot noise which, for 5 MeV alpha particles, is approximately $250 e^-$, or 0.4% .

In addition, particle hits in the periphery of each pixel will be partially collected, as shown in Fig. 3. Only hits in the region under the reset gate will be partially collected because hits in the drain region surrounding the diode will be collected by the power supply and not sensed. However, this region has an area equal to 45% of the area of the diode itself. This is a fundamental property of a small pixel size with a large perimeter to area ratio. Hits in other regions of the circuit, such as the amplifiers, multiplexer and busses will cause very small signals because of the high capacitance and low impedance of these nodes.

Finally, there are several other characteristics relevant to active pixel sensors, such as dynamic range, speed of operation, power consumption, and linearity. While we have not investigated the nonlinearity experimentally, it is expected to be 10% , coming from the variation of the diode capacitance with voltage. In principle, it can be calibrated.

11. ANTICIPATED RADIATION EFFECTS

A. Introduction

Various radiation effects can be anticipated, based on similarities to other CMOS devices. These expectations, coupled with the performance characteristics described in the previous section drive the choices of radiation testing.

Total dose radiation effects in CMOS devices can be divided into two broad classes: charge trapping and interface state generation. The mechanisms of these effects are quite complex, and have been studied in detail by many authors [7]. In addition, although we have not studied it experimentally, we discuss the anticipated effects of proton displacement.

B. Trapped Hole Effects

In simplified terms, charge trapping involves the trapping of radiation induced holes in the oxide. This occurs in both field oxides and gate oxides, and results in a negative shift in the threshold voltage. The amount of charge trapped, and hence the threshold shift, is a function of electric field, temperature, transistor polarity and radiation type. Annealing after radiation may release the trapped holes, undoing some of the threshold shift.

The simplest effect of trapped charge is just a threshold voltage shift, tending to turn n-channel transistors on and p-channel transistors off. The effects on the circuit can be predicted easily by simulation, with reference to Figure 2. An important consequence of this threshold shift is a change in the source follower load currents. This can, of course, be avoided by use of current mirrors to supply the VLN and VLP voltages. The DC output levels and dynamic range are also affected, but the changes are not simple to estimate, due to the opposing effects on the source followers and loads. Also, if the threshold shift varies from transistor to transistor, the offset FPN will be increased.

As the threshold voltage of n-channel transistors decreases with dose, their subthreshold leakage increases. A more serious problem, for non-hardened processes such as this, occurs when the threshold shift results in inversion of the field oxide or bird's beak region around n-channel transistors. The resulting source-drain leakage will increase the supply current and eventually cause functional failure. At lower levels, it may affect the functioning of the column multiplexer. Even the lowest level leakage would cause problems in the pixel, probably manifesting itself in noise and nonlinearity. It was for this reason that the design measures in Section II-D were taken.

Finally, it has been reported [8] that the presence of trapped charge can result in an increase in the 1/f noise, particularly for n-channel transistors. The magnitude of noise increase is unknown, but it could degrade the performance of the CPS32.

C. Interface State Effects

The generation of interface states is an even more complicated a subject than hole trapping. Due to their energy states in the silicon bandgap, they function as generation-recombination centers, with states near mid-gap being the most effective. When interface states are located in a depletion region, they act as sources of dark current.

Increased dark current is expected to be the dominant radiation effect in active pixel sensors, leading to increased shot noise. Variability in the added dark current will also lead to increased FPN.

The depletion region in a photodiode device, such as the CPS32, intersects the surface only around the periphery of the diode, so the dark current due to interface states is **expected** to scale with the perimeter of the device. In contrast, in a CCD or photogate APS the depletion region covers the entire detector area. Thus, photodiode devices may be expected to have a lower total dose induced dark current than photogate devices. The advantage of this choice diminishes for small pixels, however, as the perimeter-to-area ratio increases with decreasing pixel size.

Like hole trapping, the formation of interface states depends on electric field, temperature and transistor type, with interface state densities reportedly lower for p-channel device than for n-channel devices [7]. This was the primary reason for the choice of a p-channel pixel. Interface states are also reported to concentrate in regions of high mechanical stress, such as at the edge of field oxide, leading to the choice of the fully enclosed diode design.

Unlike trapped holes, interface states can not generally be annealed out at device-compatible temperatures. Indeed, during annealing, the process of removing trapped holes appears to result in the creation of interface states. This causes a "reverse annealing" effect in CCDs, where the dark current increases with annealing after radiation [9]. A similar effect is expected for active pixel sensors.

Other effects of interface states include a reduction in the sub-threshold slope, and a reduction of surface mobility, which results in lower transistor transconductance. The first of these can be a serious problem, aggravating the subthreshold leakage. The reduction of transconductance is a minor problem that can be evaluated by circuit simulation.

D. Proton Effects

Protons, in addition to producing total dose damage in the oxide, also create displacement damage in the bulk silicon. The rate of displacement production is a fundamental property of the interaction between high energy protons and silicon, and is therefore not very sensitive to technological variations. As a result, displacement damage effects in CCDs can be extrapolated to APS.

Displacement damage in the depletion region produces dark current, and a damage factor of $2.810 \cdot 10^{-1} \text{ nA/p}^+$ has been reported for CCDs irradiated with 10 MeV protons [10]. This can be usefully expressed as $0.05 \text{ nA/cm}^2/\text{krad}$, since 10 MeV protons are a good representative of a shielded proton spectrum. A similar value may be expected for the APS. Loss of red response due to displacement damage in the neutral region is not a problem for the CPS32, since the collection volume is small.

Note that the APS is not subject to the degradation of charge transfer efficiency (CTE) which besets CCDs because the APS is not a charge transfer device. This may be important in certain applications, such as star tracking.

E. Summary of Anticipated Radiation Effects

In summary, we expect that the main radiation effect is an increase in dark current, with the associated increase in shot noise and fixed pattern noise. Dynamic range and read noise may be affected, with possible leakage of reset and multiplexer transistors. We expect ultimate functional failure due to inversion of the field oxide, but the performance degradation is likely to be severe well before this point.

IV. RADIATION TEST RESULTS

A. Test Conditions

Irradiations were performed on two devices using the JPL Co⁶⁰ gamma ray source at a dose rate of 10 rad/sec in a standard Pb/Al box. The irradiations were performed at room temperature under dynamic bias, and testing was completed within a few hours, although testing performed several days later showed no change. The devices were tested at dose levels of 1, 3 and 10 krad (10, 30 and 100 Gy).

Room temperature exposure was chosen for convenience, and because the CPS32 is to be operated at near room temperature. As indicated, exposure temperature can affect the hole trapping and interface state generation processes. In particular, at cryogenic temperatures the hole trapping is greatly accentuated, while interface state generation is eliminated. This is one of the distinguishing differences between the APS and the infrared MUX. Dynamic bias was chosen as being representative of operation. Unbiased exposure is expected to be more benign.

Post-irradiation measurements, performed at room temperature, included dark current, flat field illumination, read noise, conversion gain, fixed pattern noise and dynamic range. V_{TN} and V_{TP} were measured using the pFET dosimeters and the load transistor of the output amplifier. Dark current, read noise and fixed pattern noise were also measured in an oven at temperatures of -25°C, 0°C and +25°C. Equilibration of the device temperature with the air required 20 minutes, as demonstrated by monitoring of the dark current, and the accuracy of the oven temperature is believed to be better than 1°C. Alpha particle measurements were made with an Am²⁴¹ source after the 10 krad level.

For the work described here, the clock signals were obtained from a digital output board connected to a computer, operating at 40 kHz. The analog output of the CPS32 was buffered by a low noise amplifier, with a gain of 1x or 10x, and digitized by a 13-bit ADC with a resolution of 1 mV. In the 10x mode the data acquisition system input-referred noise was -150 μV. All measurements used correlated double sampling.

B. Threshold Shift

The threshold voltage shifts were $\Delta V_{TN} = -1.3 \text{ mV/krad}$ and $\Delta V_{TP} = -2.6 \text{ mV/krad}$, consistent with other measurements we have made on this process. The dynamic range, initially -1.4 V, decreased 2.5 mV/krad. No evidence of subthreshold leakage was seen, and the supply current remained below our measurement threshold of 0.6 mA. These changes are too small to have any practical effect.

The pixel-to-pixel variation of the relaxed reset level, i.e. the fixed offset FPN, was quite large, with a standard deviation $\sigma = 90 \text{ mV}$. However, this component of FPN is removed by correlated double sampling and doesn't affect the performance. The shift of the relaxed reset level with radiation was quite uniform across the array, with a standard deviation less than 2.5 mV. This is insignificant compared to the original variability within the frame, and demonstrates that the threshold shifts do not vary from pixel to pixel.

C. Dark Current

As expected, the dark current increased dramatically with radiation. We have normalized dark current to diode area, rather than to the pixel area, since photocurrent should also scale with diode area. Scaling with pixel area would yield a dark current -5x lower. As pointed out in Section III, we actually expect the total dose induced dark current to scale with the diode perimeter, rather than the area

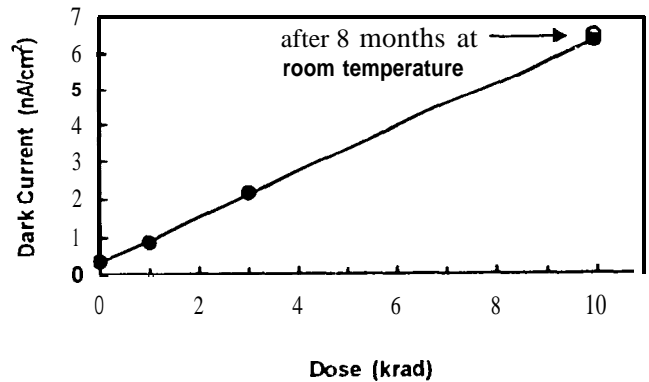


Figure 4: The dark current at 25°C as a function of dose

The dark current increased linearly with dose, as shown in Figure 4, and was thermally activated, Figure 5 shows a fit of the entire data set over dose and temperature using the simple equation:

$$I_{dark} = I_0 (1 + KD) e^{-E_a/kT} \quad (1)$$

where I_0 is the initial dark current, K is a damage factor, D is the dose, E_a is an activation energy, k is Boltzmann's constant, and T is the absolute temperature.

The extracted parameters are:

Initial dark current	0,33 nA/cm ²	(25°C)
Dark current increase	0,55 nA/cm ² /krad	(25°C)
Activation energy	0.50 eV	

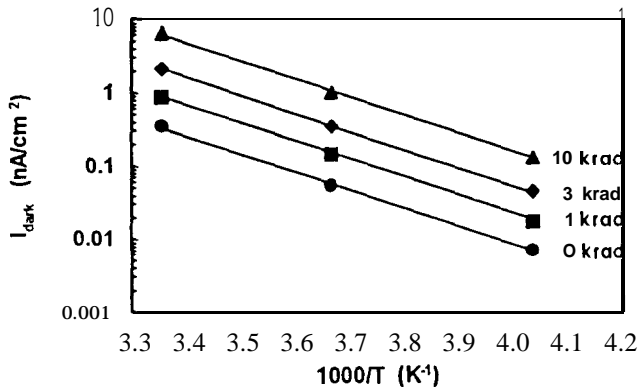


Figure 5: The dark current as a function of dose and temperature.

The activation energy is, as usual, approximately half the bandgap. This is also typical for photodiodes and CCDs. Because of this thermally activated behavior, the dark current performance can be quickly recovered by cooling. The magnitude of the dark current increase is similar to what might be expected for a non-MPP CCD [10]. An additional measurement, made after 8 months of storage at room temperature, showed a small increase in dark current, perhaps as a result of reverse annealing [9].

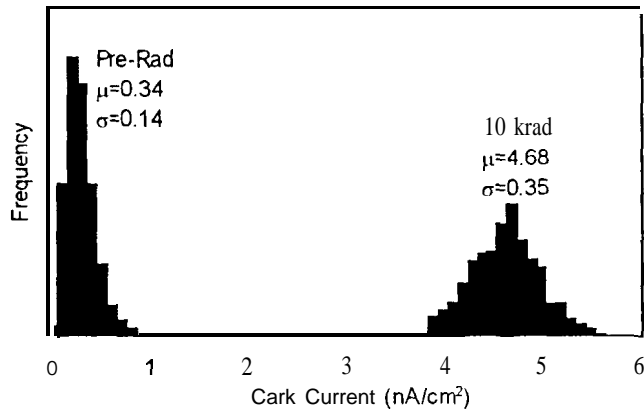


Figure 6: The 25°C dark current distribution, normalized to the diode area.

Figure 6 shows the histogram of the dark current before irradiation, and after 10 krad. The initial distribution is quite broad, in a relative sense, with the ratio of the standard deviation to the mean being $\sigma/\mu=40\%$. After 10 krad, the absolute distribution is broader, producing a noticeable fixed pattern noise, but the relative variation is only 7%. Considering the 1 krad and 3 krad measurements, it is found that the variance increases linearly with dose.

D. Noise and Conversion Gain

The read noise and conversion gain were measured by the mean-variance method, i.e. as the intercept and slope of the variance against the mean as the illumination level was changed, The variance was taken across ten frames and was pooled over all the pixels, **after** subtracting the frame averages to remove the effect of variations in integration time and fluctuations in the light level. A conversion gain of $2.4 \mu\text{V}/e^-$ was obtained, consistent with estimates of the diode capacitance, while the read noise was $\sim 100 e^-$. Neither value changed measurably over radiation or temperature.

E. Random Telegraph Signals

In the course of measuring the noise levels, we observed that the noise level for the dark current, using the pooled variance described above, increased rapidly with integration time, far in excess of the shot noise. A closer examination showed that a few pixels with very high variances were responsible. Time series measurements for these pixels showed the Random Telegraph Signal (RTS) behavior shown in Figure 7. The rapid increase in pooled variance is a result of the fact that the step size is proportional to the integration time. Hence, the variance due to RTS increases with the square of the integration time, in contrast to the variance due to shot noise, which is linear with integration time. Additionally, the number of pixels undergoing RTS transitions increased as the total measurement time increased.

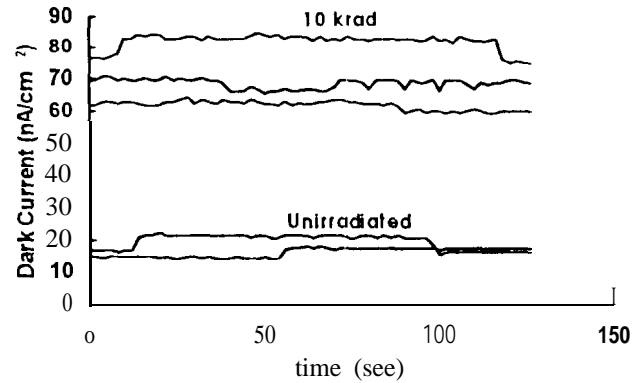


Figure 7: Random Telegraph Signals seen in the dark current of selected pixels.

Unfortunately, the Random Telegraph Signals were not identified until after radiation, so it was **difficult to determine** the effect of radiation on them. However, the overall variances of irradiated and unirradiated parts roughly matched as a function of integration time, and the fraction of pixels showing RTS behavior was $\sim 10\%$ in both cases. This seems to indicate that the RTS did not increase with radiation,

Similar Random Telegraph Signals have been observed in proton irradiated CCDs [11], and are attributed to defects with two configurations, closely spaced in energy. Although

we have not yet had the opportunity to study the RTS on the CPS32 in detail, it appears to differ from that reported for CCDs. First, it is present on unirradiated devices, although this could be evidence of residual processing damage. Second, the time scale for the transitions is tens of seconds for the CPS32, as compared with hours for the CCDs. Finally, the transition amplitude appears to be larger for the CPS32, several femtoamps, in contrast to tenths of femtoamps for the CCDs. These differences lead us to suspect that the responsible defects may be interface defects at the gate oxide, rather than the bulk defects presumed to cause the similar effect in CCDs.

Random Telegraph Signals can create a serious noise problem for applications with long integration times, such as imaging, because it makes it impossible to subtract the dark current FPN.

E. Alpha Spectra

Particle detection performance was evaluated by recording the alpha particle spectrum from an Am^{241} source in vacuum, as shown in Figure 8. These spectra represents 2000 frames of 100 ms integration time. Correlated double sampling was used to remove kTC noise and the histogram was computed from the absolute value of the difference of consecutive pairs of frames. This approach removes the offset and dark current FPN component, and is also insensitive to Random Telegraph Signals, except for a single count when a transition occurs within a pair of frames.

Am^{241} alpha particles have an energy of 5.4 MeV and an LET of $0.59 \text{ MeV}\cdot\text{cm}^2/\text{mg}$, and, as shown, produce a signal of 140 mV or $-58,000 e^-$ in the CPS32. We therefore compute a sensitivity of $240 \text{ mV}/(\text{MeV}\cdot\text{cm}^2/\text{mg})$. The 1400 mV dynamic range then corresponds to an LET of $6 \text{ MeV}\cdot\text{cm}^2/\text{mg}$.

Several features are evident in Figure 8. First, the low read noise is evident in the fact the nearly two million dark counts are confined to the first 10 channels. Second is the presence of the peripheral hits, which are represented by the uniform background from zero to the peak. As predicted, they number about half the direct hits. Finally we observe that the peak is rather broad, with $\sigma/\mu=7\%$. It was originally believed that this was due to spread in the source, but a measurement with a surface barrier diode, also shown in Figure 8, demonstrated that this was not the cause. Likewise, the source was small and far enough from the detector to rule out angular effects, although these will occur in space. We now believe the cause is probably pixel-to-pixel sensitivity variation, although this is twice the variation seen in flat field optical illumination.

Since the technique for obtaining good alpha spectra was not developed until after radiation was completed, it is somewhat difficult to judge the effect of radiation. Comparing the alpha spectra of irradiated and unirradiated devices, the differences are small. The alpha peak for the

irradiated device is shifted slightly (3%) to the left, but this is probably the result of gain variations. The peak for the irradiated device is also somewhat noisier and wider. Most interesting, however, is that the peripheral hits are down to only 35% of the direct hits. This may again be part-to-part variation, or it may represent an increase in the surface recombination velocity under the reset gate due to interface states.

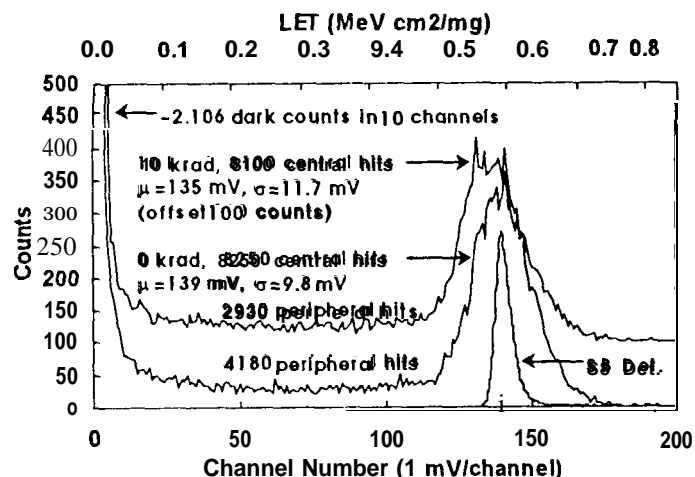


Figure 8: Am^{241} alpha spectra recorded with the CPS32. The Am^{241} alpha particle has an energy of 5.4 MeV and an LET of $0.59 \text{ MeV}\cdot\text{cm}^2/\text{mg}$. 0 krad and 10 krad curves are for different parts.

V. DISCUSSION

As seen from the alpha particle testing, the spectrometry performance of the CPS32 is limited by peripheral hits and pixel-to-pixel variability, issues unrelated to radiation effects. It is, therefore, not surprising that there was no clear degradation of spectrometry performance with radiation. We will therefore assess the radiation effects, not against spectrometry performance, but against signal-to-noise ratio.

First, it is important to note that, up to the 10 krad dose tested, the CPS32 remained entirely functional. The dominant total dose effect was an increase in the 25°C dark current of $0.58 \text{ nA}/\text{cm}^2/\text{krad}$. This is an order of magnitude larger than the increase expected due to displacement damage, confirming the assertion that the total dose effects dominate. Although the dark current at 10 krad is 20 times its initial value, it still amounts to only $4500 e^-/\text{pixel}$ for a 100 ms integration time. The shot noise on this value is $65 e^-$, comparable to the noise floor of the device. Thus, the dark current would not be expected to degrade the device in any case.

The dark current FPN, which would be relevant to imaging devices, is $300 e^-$ for the same conditions. Furthermore, this FPN is proportional to integration time, whereas the shot noise increase with the square root of integration time. Thus, for imaging, the dark current FPN is likely to be the main performance limitation.

Dark current has the additional effect of reducing dynamic range by leading to saturation. At the 10 krad dark current, saturation will occur in 13 sec.

Because the dark current is thermally activated, the dark current problems will be aggravated at higher temperatures and ameliorated at lower temperatures. In particular, for the STRV-2 application, the dark current will be 8 times greater than the stated values at +60°C, while at -40°C it will be 200 times less. Clearly, the usability of these devices will remain to much higher doses at the cooler temperatures.

We have shown that the dark current performance can be recovered by modest cooling, and that effects such as read noise and dynamic range are not significantly affected. It appears that the ultimate dose limitation for the CPS32 will be due to inversion of the field oxide, and because of the radiation hardening features in the CPS32 design, only the digital portions of the circuit are susceptible. Our previous experience with this process indicates that it will function for digital circuits to greater than 100 krad.

VI. CONCLUSIONS

CPS32 charged particle spectrometer chips were total dose tested to 10 krad. The major degradation of these devices, a linear increase in dark current, does not interfere with particle spectrometry operation. The dark current rates and threshold shifts suggest that the device may be useful to doses as high as 100 krad, given the short integration time used for particle spectrometry. The Random Telegraph Signals that give rise to the excess noise in the dark current do not appear to be affected by the radiation. These results also indicate that imaging APS chips will suffer significant degradation, particularly due to dark current fixed pattern noise, but should remain useful for bright scenes to doses above 10 krad, especially with moderate cooling.

ACKNOWLEDGMENTS

The CPS32 was designed and provided by Robert Nixon. We also acknowledge useful discussions with Bedebrata Pain and Gary Swift. This work was funded by NASA Code Q.

REFERENCES

- [1] G.A. Soli, H.B. Garrett and E.R. Fossum, "CMOS Charged Particle Spectrometers", IEEE Trans. Nuc.Sci., vol. 43, pp. 1516-1520, June 1996.
- [2] M.G. Buehler, B.R. Blaes, G.A. Soli and G.R. Tardio, "On-Chip p-MOSFET Dosimetry" IEEE Trans. Nuc. Sci., vol. 40, pp. 1442-1449, December 1993.
- [3] R.H. Nixon, S.E. Kemeny, B. Pain, C.O. Staller and E.R. Fossum, "256X256 CMOS Active Pixel Sensor Camera-on-a-Chip", IEEE J. Solid State Circ., vol. 31, pp.2046-2050, December 1996.
- [4] E. R. Fossum and B. Pain, "Infrared Readout Electronics for Space-Science Sensors: State of the Art and Future Directions", Infrared Technology XLX, Proc.SPIE, vol. 2020, p.262, 1993.
- [5] J.D. Garnett and W.J. Forrest, "Multiply Sampled Read Limited and Background Limited Noise Performance", Infrared Detectors and Instrumentation, Proc.SPIE, vol. 1946, pp.395-404, 1993.
- [6] H. Zulliger and D. Aitken, "Fano Factor Fact and Fallacy", IEEE Trans. Nuc. Sci., vol. 17, p.197, 1970.
- [7] See, *for example*: T.P. Ma and P.V. Dressendorfer, Ionizing Radiation Effects in MOS Devices and Circuits, New York; John Wiley and Sons, 1989.
- [8] T.L. Meisenheimer and D.M. Fleetwood, "Effect of Radiation-Induced Charge on 1/f Noise in MOS Devices", IEEE Trans. Nuc. Sci., vol. 37, pp.1696-1702, December 1990.
- [9] J.C. Boudenot and B. Augier, "Total Dose Effects on CCDs - Reverse Annealing Phenomena", Proc. ESA Electr. Comp. Conf., Noordwijk, NL, 12-16 Nov., 1990, ESA SP313 (March 1991), pp.319-324.
- [10] G.R. Hopkinson, C.J. Dale and P.W. Marshall, "Proton Effects in Charge-Coupled Devices", IEEE Trans. Nuc. Sci., vol. 43, pp.614-627, April 1996.
- [11] I.H. Hopkins and G.R. Hopkinson, "Further Measurements of Random Telegraph Signals in Proton Irradiated CCDs", IEEE Trans. Nuc. Sci., vol. 42, pp.2074-2081, December 1995.